ORGANOMETALLICS

pubs.acs.org/Organometallics Article

# Competition between Ring-Closing Migratory Insertion Polymerization and Monomer Cyclization

Aaron Leung, Jing Kang, Yuanting Cai, Weiwei Chang, Kun Liu, Haiping Xia, and Xiaosong Wang*

Cite This: *Organometallics* 2020, 39, 2991−2997 Read Online

ACCESS | Metrics & More | Article Recommendations | Supporting Information

**ABSTRACT:** Migratory insertion polymerization (MIP) of $^{P}$FpR [$^{P}$Fp = $(PPh_2(CH_2)_3Cp)Fe(CO)_2$, R = $(CH_2)_4CH{=}CH_2$ or $(CH_2)_5CH_3$] (**1**) involved competitive MIP ring-closing polymerization and monomer cyclization (MC), producing P($^{P}$FpR) macrocycles (**2**) and $^{P}$FpR rings (**3**), respectively. MC, generating **3**, occurred at the early stage of MIP, while the growing polymer chains exclusively underwent ring-closing cyclization without producing any linear analogues. The effect of solvent, temperature, and the concentration of **1** on the competition between the ring-closing MIP and MC was investigated. **3** was synthesized as the only product in THF with a low concentration of **1** (1 wt %), while the ring-closing MIP predominated under the condition at 60 °C with a high concentration of **1** in THF (>70 wt %), resulting in **2** with $M_n$ up to 17 500 g/mol. This effective synthesis of ring molecules is attributed to the piano-stool coordination geometry and the low rotation barrier of Cp−Fe bond and will facilitate further exploration of ring molecules as functional materials and supramolecular building blocks.

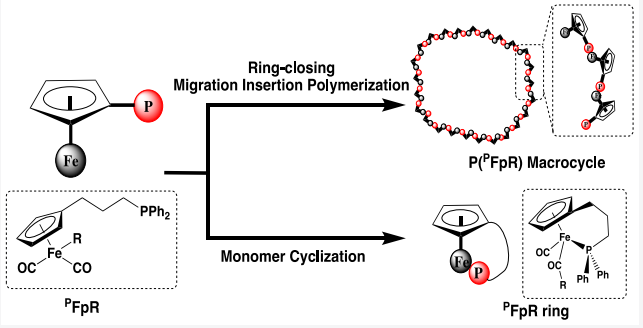


## INTRODUCTION

Synthesis of cyclic compounds has been an active research topic, inspired by the unique shape and functions of cyclic biomolecules in living organisms, such as cellulose, peptide, and DNA, and so on.[1] Consequently, many cyclic compounds with sizes ranging from 3-atom rings to cyclic polymers or macrocycles have been synthetically produced.[2−4] However, the synthesis of these cyclic compounds, especially macrocycles, requires tedious after-reaction purification steps and is yet to be improved.[1,5]

The synthesis of organometallic ring molecules has been explored for possible new functions derived from the metal elements.[6−11] Nonlinear metal coordination geometries are an advantage for the cyclization. Cyclopentadienyl (Cp) metal carbonyl complexes bearing a pendant phosphorus have a piano-stool coordination geometry and can undergo an intramolecular phosphorus−metal coordination producing ring molecules.[12,13] In addition to the small rings, cyclic macromolecular structures have also been made via metal coordination, but the resultant metal-coordinated structures are usually rigid without viscoelastic properties[14] characteristic of polymer materials. The techniques, developed for the synthesis of organic cyclic polymers including intramolecular end-group coupling for ring-closure and ring-expansion polymerization,[5] are not applicable for the synthesis of organometallic macrocycles.

Ring-closing polymerization for the synthesis of organometallic macrocycles with viscoelastic properties has been discovered for two systems. The ring-opening polymerization of silicon-bridged [1]ferrocenophanes using 4,4′-dimethyl-2,2′-bipyridine ($Me_2$bpy) as initiator produces polymer chains with propagating active species of Cp anions. The backbiting of Cp anions replaces the $Me_2$bpy ligands generating polyferrocenylsilane (PFS) macrocycles.[4] We have previously developed migratory insertion polymerization (MIP)[15] and reported the MIP in bulk of $^{P}$FpR (**1**) [$^{P}$Fp = $(PPh_2(CH_2)_3Cp)Fe(CO)_2$, R = $CH_3$ or $(CH_2)_5CH_3$], resulting in a new type of iron−carbonyl macrocycles P($^{P}$FpR), **2**.[16] The ring-closing process is facilitated by the nonlinear piano-stool metal coordination geometry and the conformational flexibility of the polymer chain due to the low rotation barrier of the Cp−Fe bond in the backbone.[16−18] During the synthesis of **2**, a small fraction of unknown molecules was produced and removed by a precipitation process.[16] It appears that the MIP involves competitive reactions for two products. This competition is not yet understood.

Herein, we report the MIP of $^{P}$FpR (**1**) [**1a**: R = $(CH_2)_4CH{=}CH_2$; **1b**: $(CH_2)_5CH_3$], which involves two competing reactions: ring-closing MIP and monomer cyclization (MC). By adjusting the conditions, either P($^{P}$FpR)

Received: May 18, 2020
Published: August 7, 2020







https://dx.doi.org/10.1021/acs.organomet.0c00346
*Organometallics* 2020, 39, 2991−2997

macrocycles (**2**) or $^{P}$FpR rings (**3**) were exclusively prepared in excellent yields (Scheme 1).

**Scheme 1. Two Routes for the Migratory Insertion Reaction (MIR) of 1: Ring-Closing MIP Yielding 2 without Linear Analogues and MC Yielding 3**

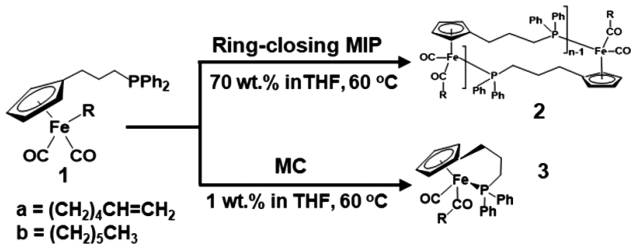


## RESULT AND DISCUSSION

**Bulk MIP of 1 and Characterization of the Resultant 2.** The MIP of **1** was performed in bulk at 105 °C. The polymerization behavior for the two monomers (**1a** and **1b**) is identical, because the pendent R groups are not involved in the migratory insertion reaction of the Fp group. As has been reported,[16] the polymerization of **1b** generated a small fraction of unknown products in addition to **2b**, which is illustrated by the $^{31}$P NMR ($CDCl_3$) spectrum of a crude product (Figure 1a). As shown in Figure 1a, the two signals at 72.3 and 71.5

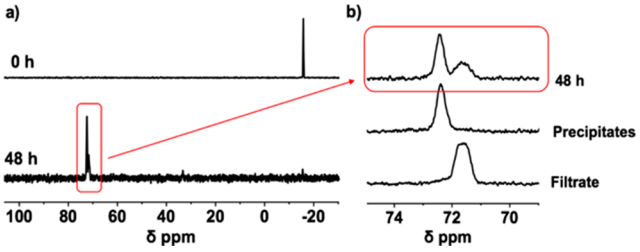


**Figure 1.** (a) $^{31}$P NMR ($CDCl_3$) spectra of **1b** before and after MIP in bulk at 105 °C for 48 h. (b) Partial $^{31}$P NMR spectra for the crude products and the separated components.

ppm are attributed to **2b** and the unknown product, respectively.[16] To remove the unknown product, we added hexane to a THF solution of the crude products to precipitate **2b**. The hexane-soluble product was collected in the filtrate, which shows one signal at 71.5 ppm in the $^{31}$P NMR spectrum (Figure 1b).

**2b** has been fully characterized as a macrocycle in our previous work.[16] The $^{1}$H and $^{31}$P NMR spectroscopies of **2a** (Figure 2), like those for **2b**, only show the Cp group (4.0 ppm in Figure 2a) and the coordinated phosphorus (72.3 ppm in Figure 2b) in the main chain. The absence of detectable NMR

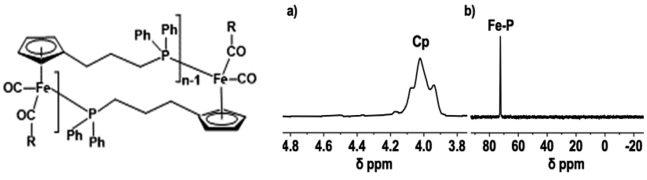


**Figure 2.** (a) Partial $^{1}$H NMR ($CDCl_3$) spectrum and (b) $^{31}$P NMR ($CDCl_3$) spectrum for **2a**.

signals for the end-groups is attributed to the formation of a cyclic structure.[16] To further confirm the structure of **2a**, transmission electron microscopy (TEM) was subsequently performed. The TEM sample of **2a** (5 mg/mL in THF) was prepared by adding a drop of the solution onto a carbon-coated copper grid. As seen in Figure 3, rings with diameters of

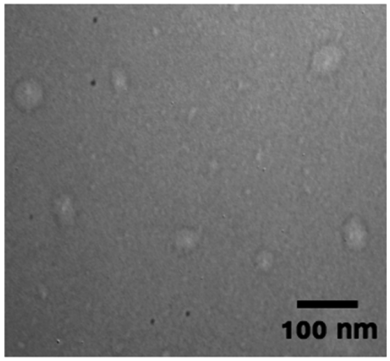


**Figure 3.** TEM image of **2a** macrocycles. The image was taken after exposing the sample to the electron beam for a few minutes. Scale bar is 100 nm.

ca. 20−30 nm and ca. 5−10 nm were observed. The contrast was caused by the breakage of the carbon substrate in the center of the ring molecules after exposing the grid to electron beams for a few minutes.[16] By comparing the circumference of the larger rings with the size of the monomers, the degree of polymerization (DP) for the macrocycle ranges from 40 to 60. The absolute molecular weight (MW) of the sample as measured by GPC (triple detectors) is ca. 23 000 g/mol, corresponding to the DP of 49, which matches with the value estimated from the TEM image. The GPC trace tails toward the higher retention times with a large polydispersity index (PDI) of ca. 1.5, which is in line with the TEM observation. Matrix-assisted laser desorption/ionization time-of-flight mass spectrometry (MALDI-TOF) experiments of **2a** and **2b** were attempted with or without matrix (Table S1). However, no meaningful results were obtained. The technique for the characterization of **2** remains to be a matter of future research.

**Characterization of 3.** The chemical structure for the hexane-soluble product, collected in the filtrate, was unknown and is, therefore, fully analyzed by X-ray crystallography, FT-IR, and NMR spectroscopies; mass spectrometry (MS); and element analysis. Yellow crystals were obtained from a slow solvent evaporation of saturated hexane solutions, whose X-ray diffraction reveals a monoclinic crystal system with a $P21/c$ space group (Table S2). As shown in Figure 4, **3** is a $^{P}$FpR ring that is formed via an intramolecular Fe−P coordination with the bond length of 2.16 Å for **3a** and 2.17 Å for **3b**. Migratory insertion MC of **1** (Scheme 1) accounts for the formation of ring structures, as the Fe−P coordination results in the conversion of one terminal CO to acyl CO group. The acyl CO group is also indicated by the FT-IR absorption at 1599 $cm^{-1}$ (Figure 5a)[16] and the chemical shift at 279.42 ppm in the $^{13}$C NMR spectrum (Figure 5b).[16] The masses for **1** and **3** is expected to be the same upon MC (Scheme 1). The electrospray ionization MS experiment shows a molecular ion ($MH^+$) peak at 489.16 $m/z$ for **3b** ($C_{28}H_{33}FeO_2P$), which matches with the calculated theoretical MW of **1b** for 488.38 $m/z$. The elemental analysis of **3b** also shows a good


https://dx.doi.org/10.1021/acs.organomet.0c00346
Organometallics 2020, 39, 2991−2997

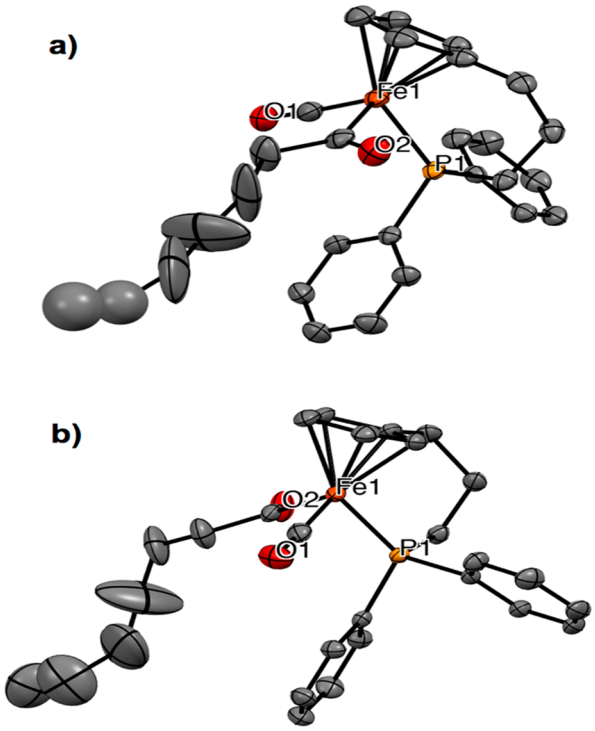


**Figure 4.** (a) ORTEP drawings (30% probability ellipsoids) for the molecular structures of **3a** and (b) **3b**. Hydrogen atoms are omitted for clarity.

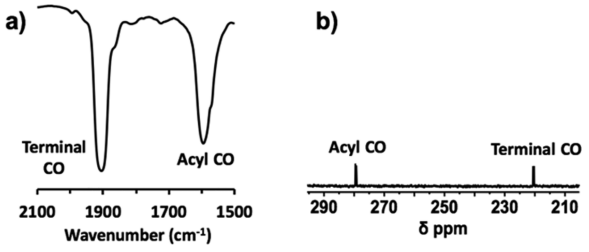


**Figure 5.** (a) Partial spectra of FT-IR and (b) $^{13}C$ NMR ($CDCl_3$) for **3a**.

agreement with the theoretical values of C and H. **3a** was also characterized in the same manner.

**3** was further characterized by $^{1}H$ and $^{13}C$ NMR spectroscopies. As shown in Figure 6a, the $^{1}H$ NMR spectrum of **3a** reveals three signals between 7.16 and 7.62 ppm and four signals between 3.8 and 4.8 ppm, which are assigned to the protons of the two phenyl groups and the Cp group, respectively.[16] The appearance of the four Cp proton signals indicates that their chemical environments are different from each other due to the presence of the Fe stereocenter as a result of the cyclization.[19,20] The chemical shifts at 5.68 and 4.86 ppm, with the integration ratio of 1:2, represent the vinyl protons $H_h$ and $H_i$ respectively. In the $^{13}C$ NMR spectrum of **3a** (Figure 6b), the peaks at 73.1−99.3, 127.8−138.1, 220, and 280 ppm are assigned to the 5 Cp carbons, 12 phenyl carbons, the terminal CO carbon, and the acyl CO carbon, respectively.[15,16] The signal at 65.5 ppm is assigned to the $\alpha$ carbon ($C_d$) next to the electron withdrawing acyl CO group, which causes the chemical signal of $C_d$ to appear at the lower field than other $CH_2$ carbons.[15,16] Other protons and carbons (a−i) peaks in Figure 6 are also assigned and confirmed by $^{13}C-^{1}H$ HMQC and $^{1}H-^{1}H$ COSY (correlation spectroscopy) spectra (Figure S1) and $^{13}C-^{1}H$ HMQC (heteronuclear multiple quantum correlation) 2D NMR experiments (Figure S2). Multiple sets of diastereotopic protons of b−e (Figures S1 and S2) are explained by the presence of the Fe chiral stereocenter.[20] **3b** was also characterized in the same manner (Figures S3−S6).

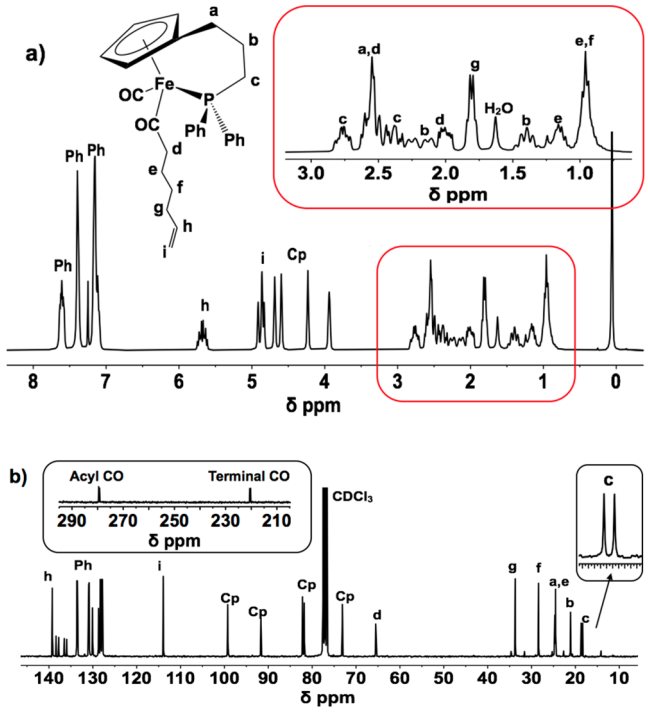


**Figure 6.** (a) $^{1}H$ NMR ($CDCl_3$) and (b) $^{13}C$ NMR ($CDCl_3$) spectra for **3a**.

**Solution MIP of 1.** The effect of solvent on the MIP of **1b** in solutions (50 wt %) at 60 °C was investigated. After 48 h, a sample of the crude product was dissolved in $CDCl_3$ and analyzed by $^{31}P$ NMR spectroscopy. As shown in Figure 7a,b, when the polar solvents DMSO and DMF are used, the $^{31}P$ NMR spectra of the crude products show a significant signal at 71.5 ppm, representing **3b**, aside from the signal at 72.3 ppm due to **2b**.[16] In contrast, the THF system produced a smaller

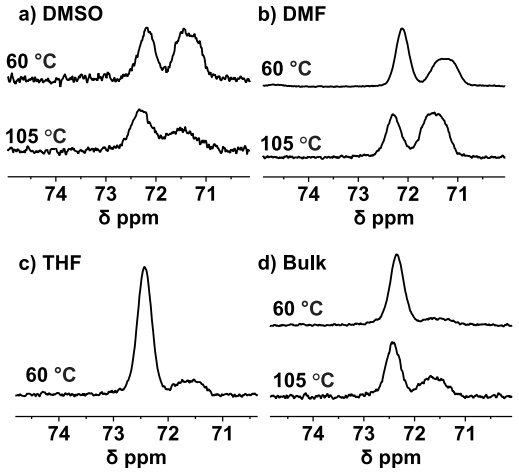


**Figure 7.** $^{31}P$ NMR ($CDCl_3$) spectra for the crude products produced via MIP of **1b** at 60 or 105 °C in (a) DMSO, (b) DMF, and (c) THF with 50 wt % **1b** and (d) in bulk.


https://dx.doi.org/10.1021/acs.organomet.0c00346
Organometallics 2020, 39, 2991−2997

amount of **3b** (Figure 7c), as indicated by the weaker intensity of the chemical shift at 71.5 ppm. The polar solvents can promote a migratory insertion reaction,[21,22] which increases the chance for the MC of **1b** before the occurrence of intermolecular reactions for the polymerization.

Time-dependent $^{31}$P NMR analysis also indicated that the MC of **1b** produces **3b** at the early stage of MIP. As shown in the $^{31}$P NMR spectra for the samples taken at various reaction intervals (Figure 8), both MIP for a chain growth and MC

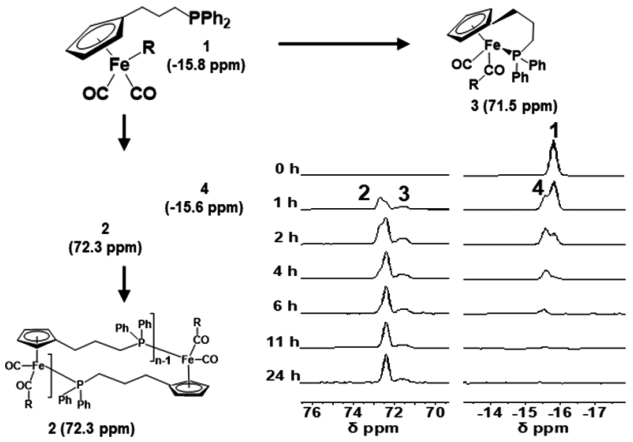


**Figure 8.** Time-dependent $^{31}$P NMR ($CDCl_3$) spectra for the MIP at 60 °C in THF with 50 wt % concentration of **3b**.

(producing **3**) occur within the first hour, as indicated by the appearance of the chemical shifts at 72.3 and 71.5 ppm (Fe−P bonds) and the chemical shift at −15.6 ppm ($PPh_2$ end-group of noncyclized oligomers, **4**).[16] This result suggests that the MIP and MC are two competing reactions. After 6 h, the monomer signal at −15.8 ppm disappears, suggesting a complete consumption of the monomers. However, the chemical shift at −15.6 ppm remains, suggesting the presence of linear polymers with phosphine end groups.[16,23,24] This end group signal (−15.6 ppm) completely vanished after 24 h, which indicates that all linear chains were cyclized.

By comparing the systems in DMSO and DMF at 60 °C, the production of **3b** in the DMSO system is particularly favored as indicated by a significant signal at 71.5 ppm in the spectrum (Figure 7a). We attributed this difference to the solvent viscosity, as DMSO is 2-fold more viscous than DMF. The high viscosity of DMSO, 1.12 cP at 60 °C,[25] may limit the mobility of the molecules, thus favoring the intramolecular MC at the early stage of the reaction. If the hypothesis is right, then the production of **3b** can be suppressed by increasing the temperature to reduce the solvent viscosity.[26] As shown in Figure 7a, a higher temperature (105 °C) substantially reduces the production of **3b** (Figure 7a). However, the MIP at 105 °C in DMF (Figure 7b) or in bulk (Figure 7d) does not suppress the MC but rather generates more **3b**. These results can be understood by the two effects caused by a higher reaction temperature: (1) reduced viscosity that suppress the MC and (2) increased reaction rate that favors the MC. The latter effect may be predominant when the MIP is performed in DMF solution, resulting in an increased possibility for the production of **3b**. For a bulk MIP, the two effects compete with each other, producing less **3b** at 105 °C (Figure 7d) as compared with the MIP in DMF at the same temperature (Figure 7b).

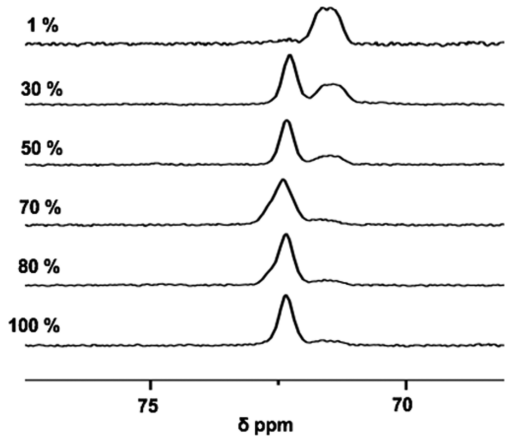


**Figure 9.** $^{31}$P NMR ($CDCl_3$) spectra of the crude product prepared by MIRs of **1a** in THF with the monomer concentrations of 1−100 wt % at 60 °C for 48 h.

The concentration effect of **1** on the competition for the production of **2** and **3** was investigated. Figure 9 illustrates the $^{31}$P NMR spectra for the crude products resulting from the MIP of **1a** (including MC or ring-closing MIP) at different concentrations in THF at 60 °C. As shown in Figure 9, when the concentration is extremely low (1 wt %), only one signal at 71.5 ppm is observed, indicating that the MC is the only reaction producing **3a**, and no ring-closing MIP occurs. By increasing the concentration, the peak intensity at 71.5 ppm decreased. It suggests that the MC is suppressed by a higher monomer concentration. It is reasonable because a higher concentration suppresses the formation of small rings.[27] For the systems with concentrations above 70 wt %, MC is significantly suppressed as the signal at 71.5 ppm is fairly weak, and **2a** becomes the major product. A higher concentration favors the intermolecular reaction to grow polymer chains, which reduces the possibility of MC. However, the growing chains eventually cyclized, producing **2**, which is attributed to the nonlinear piano-stool coordination geometry and the freely rotating Fe−Cp bonds in the backbone.[16]

The GPC analysis of the macrocycle, **2a**, produced via the MIP with the concentrations above 50 wt % (Figure S8) is summarized in Figure 10. As shown in the figure, the highest

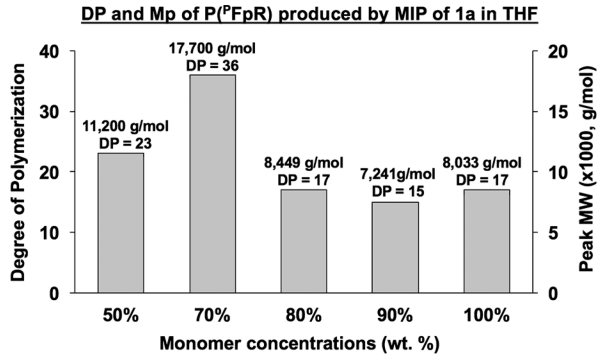


**Figure 10.** DP and peak MW ($M_p$) of P($^P$FpR) produced by MIP of **1a** in THF. $M_p$ was determined by GPC using DMF as the eluent and PS as the standards.


https://dx.doi.org/10.1021/acs.organomet.0c00346
Organometallics 2020, 39, 2991−2997

MW of **2a** was obtained at 70 wt %, with a $M_p$ of 17 700 g/mol, corresponding to a DP of 36. The lower concentration (50 wt %) results in a smaller $M_p$ (11 200 g/mol). This is reasonable as a low concentration favors intramolecular cyclization. By increasing the monomer concentration to 80 wt % or even 100 wt % (bulk), the $M_p$, however, was reduced to 7200−8500 g/mol. The smaller macrocycles produced is rationalized by the reduced mobility of the oligomers, as we observed that the reaction systems with the concentrations above 70 wt % became bulklike. The low mobility decreases the possibility for intermolecular reaction to form polymers with higher MWs.

## SUMMARY

MIP of $^{P}$FpR (**1**) involves two competing pathways of ring-closing MIP and MC, generating macrocycles (**2**) and $^{P}$FpR rings (**3**), respectively, without the contamination of linear macromolecules. **3** can be removed by a simple precipitation purification resulting **2**. On the basis of the effect of solvent, temperature and concentration of **1** on the MIP, $^{P}$FpR rings **3** can be produced exclusively via MC when the MIP of **1** with a low concentration (1 wt %) is performed in THF at 60 °C. At a high monomer concentration of **1** (>70 wt %), P($^{P}$FpR) macrocycles (**2**) are effectively produced via ring-closing MIP. **2a** is a new macrocycle containing pendent vinyl groups that can be useful for postpolymerization modification. This effective synthesis of ring molecules will facilitate our further studies to explore the properties and supramolecular chemistry of iron−carbonyl compounds.

## EXPERIMENTAL SECTION

**Materials and Instrumentation.** All experiments were performed under an atmosphere of dry nitrogen using standard Schlenk techniques unless otherwise indicated. 1-Bromohexane (98%), 1-chloro-3-iodopropane (99%), 6-chloro-1-hexene (96%), benzophenone (99%), *sec*-butyllithium solution (1.4 M in cyclohexane), cyclopentadienyl iron(II) dicarbonyl dimer ($Fp_2$, 99%), potassium (chunks in mineral oil, 98%), and sodium were purchased from Sigma-Aldrich. Chlorodiphenylphosphine (>97.0%) was purchased from Tokyo Chemical Industry CO. All chemicals were used as received unless otherwise indicated. Tetrahydrofuran (THF) was freshly distilled over sodium/benzophenone under nitrogen before use.

$^{1}$H, $^{13}$C, and $^{31}$P NMR, $^{1}$H−$^{1}$H correlation spectroscopy (COSY), and $^{13}$C−$^{1}$H heteronuclear multiple quantum coherence (HMQC) 2D NMR were recorded on a Bruker Avance 300 (300 MHz) spectrometer at ambient temperature using $CDCl_3$ as the solvent. $^{1}$H NMR chemical shifts were reported relative to the residual $CHCl_3$ signal and $^{31}$P NMR resonances were referenced to an external standard sample of 85% $H_3PO_4$.

TEM images were obtained on a TEM apparatus (Philips CM10) with an acceleration voltage of 60 kV. TEM samples were prepared by adding 10 μL of sample in THF solution on a carbon-coated copper grid. The copper grid was dried overnight at room temperature. The rings appear after exposing the grid to the electron beams for a few minutes.

Mass spectrometry was acquired by performing positive ion electrospray ionization (ESI) on a Thermo Scientific Q-Exactive Orbitrap mass spectrometer. Samples were infused at 10 μL/min in acetonitrile.

Fourier transform infrared (FT-IR) spectra were recorded on a Thermo Scientific Nicolet 5700 spectrometer with a resolution of 0.4 $cm^{-1}$.

Elemental analyses were carried out by using Vario EL cube on an elemental analyzer (Elementar).

Single crystals suitable for X-ray diffraction analysis were mounted onto the tips of glass fibers with paratone oil and transferred immediately into the cold nitrogen gas stream of the diffractometer cryostat. X-ray data were collected using Mo Kα radiation (λ = 0.71073 Å) at 200 K on a Bruker Kappa APEX II diffractometer (Madison, WI). Structures were solved using direct methods and refined by full-matrix least-squares on $F_2$ using the APEX2 package.

Gel permeation chromatography analyses were carried out using 2 instruments: (1) Viscotek VE 2001 GPC instrument equipped with PolyAnalytik SupeRes mixed bed columns and a TDA 305 triple detector array (differential refractive index, light scattering, and viscosity) using THF as the eluent. The temperature was set at 35 °C and held constant with a flow rate of 1 mL/min. Absolute MW was obtained. (2) Agilent 1100 Series GPC module equipped with two Jordi Resolve DVB medium mixed bed columns and a Waters 410 differential refractometer using DMF with 0.1% lithium chloride as the eluent. The columns were maintained at 45 °C and held constant with a flow rate of 0.9 mL/min. MW was calculated from PS standards. Both methods gave similar results.

**Preparation of Cyclopentadienyl Iron(II) Dicarbonyl Potassium (FpK), $[\eta^5\text{-}C_5H_5]Fe(CO)_2K$.** Potassium benzophenone ketyl was first prepared by stirring benzophenone (5.00 g, 27.5 mmol, 1.0 equiv) and potassium metal (1.07 g, 27.5 mmol, 1.0 equiv) in a Schlenk flask containing distilled THF (70 mL). The solution mixture was stirred overnight to ensure complete reactions. Afterward, cyclopentadienyl iron(II) dicarbonyl dimer ($Fp_2$, 5.35 g, 15.1 mmol, 0.55 equiv) was added to the solution and stirred for 2 h at room temperature to produce FpK. The FpK solution (in THF) was used directly without purification.

**Preparation of FpR, $[\eta^5\text{-}C_5H_5]Fe(CO)_2R$, R = $(CH_2)_4CH{=}CH_2$) or $(CH_2)_5CH_3$.** In a Schlenk flask containing the FpK solution (5.94 g, 27.5 mmol, 1.0 equiv), an alkyl halide, and 1-bromohexane for **a** (4.08 g, 24.7 mmol, 0.9 equiv) or 6-chloro-1-hexene for **b** (2.93 g, 24.7 mmol, 0.9 equiv) was added dropwise to the solution mixture at 0 °C. Afterward, the solution mixture was warmed to room temperature and stirred for another 2 h. After the reaction, THF solvent was removed, and the reaction crude product was filtered through Celite using hexane as the eluent. The filtrate was subsequently collected and further purified after solvent evaporation, by running a silica-gel column using hexane as the eluent. The yellow band was collected, and the hexane solvent was removed under vacuum to yield a yellow oil. For **a**, $Fp(CH_2)_4CH{=}CH_2$: Yield: 88%. $^{1}$H NMR ($CDCl_3$): 5.79 (ddt, $J$ = 17.1 Hz, 10.1 Hz, 6.8 Hz, 1H, $Fe(CH_2)_4C\mathbf{H}{=}CH_2$), 5.00−4.89 (m, 2H, $Fe(CH_2)_4CH{=}C\mathbf{H}_2$), 4.71 (s, 5H, $C_5\mathbf{H}_5$), 1.53−1.43 (8H, $Fe(C\mathbf{H}_2)_4CH{=}CH_2$) ppm. For **b**, $Fp(CH_2)_5CH_3$: Yield: 83%. $^{1}$H NMR ($CDCl_3$): 4.71 (s, 5H, $C_5\mathbf{H}_5$), 1.43−1.26 (10H, $Fe(C\mathbf{H}_2)_5CH_3$), 0.86 (3H, $(CH_2)_5C\mathbf{H}_3$) ppm.

**Preparation of $^{Cl}$FpR, $[\eta^5\text{-}Cl(CH_2)_3C_5H_4]Fe(CO)_2R$.** In a Schlenk flask containing FpR (1.0 equiv, for **a**: 3.55 g, 13.5 mmol; or for **b**: 3.68 g, 14.1 mmol) in distilled THF (100 mL), *sec*-butyllithium (1.4 M in cyclohexane; 1.5 equiv; for **a**: 14.5 mL, 20.3 mmol; or for **b**: 15.2 mL, 21.2 mmol) was added dropwise at −78 °C and stirred for 15 min. 1-Chloro-3-iodopropane (1.7 equiv; for **a**: 2.5 mL, 23.0 mmol; or for **b**: 2.6 mL, 24.1 mmol) was then added to the solution mixture at −78 °C while stirring. The solution was warmed to room temperature and stirred for 1.5 h. THF solvent was removed after the reaction, and the crude product was filtered through Celite using hexane as the eluent to remove LiI salts. The filtrate was collected and further purified by silica-gel column chromatography using hexane as the eluent. Subsequently, one large yellow band was separated. A mixture of hexane and dichloromethane (3:1 v/v) was then used as the eluent to further separate the yellow band. Afterward, two yellow bands were separated, and the second yellow band was collected as the product. The solvent was removed under vacuum, yielding a yellow oil product. For **a**, $^{Cl}Fp(CH_2)_4CH{=}CH_2$: Yield: 53%. $^{1}$H NMR ($CDCl_3$): 5.80 (ddt, $J$ = 16.8 Hz, 10.2 Hz, 7.0 Hz, 1H, C**H**=$CH_2$), 4.94 (m, 2H, CH=C**H**$_2$), 4.60 (s, 2H, $C_5\mathbf{H}_4$), 4.56 (s, 2H, $C_5\mathbf{H}_4$), 3.55 (t, 2H, C**H**$_2$Cl), 2.39 (t, 2H, $(C_5H_4)C\mathbf{H}_2$), 2.00 (m, 2H, $CH_2C\mathbf{H}_2CH_2Cl$), 1.42 (m, 2H, $FeC\mathbf{H}_2$), 1.26 (m, 6H, $CH_2(C\mathbf{H}_2)_3CH{=}CH_2$) ppm. For **b**, $^{Cl}Fp(CH_2)_5CH_3$: Yield: 42%.


https://dx.doi.org/10.1021/acs.organomet.0c00346
Organometallics 2020, 39, 2991−2997

$^1$H NMR ($CDCl_3$): 4.59 (s, 2H, $C_5H_4$), 4.55 (s, 2H, $C_5H_4$), 3.55 (t, 2H, $CH_2Cl$), 2.40 (t, 2H, $(C_5H_4)CH_2$), 1.95 (q, 2H, $CH_2CH_2CH_2Cl$), 1.41 (m, 2H, $FeCH_2$), 1.26 (m, 8H, $FeCH_2(CH_2)_4CH_3$), 0.87 (m, 3H, $(CH_2)_5CH_3$) ppm.

**Preparation of $^P$FpR, [$\eta^5$-Ph$_2$P(CH$_2$)$_3$C$_5$H$_4$]Fe(CO)$_2$R, 1.** In a Schlenk flask containing $^{Cl}$FpR (1.0 equiv; for **a**: 2.3 g, 6.8 mmol, or for **b**: 2.5 g, 7.4 mmol) in distilled THF (100 mL), sodium diphenylphosphide solution (0.5 M in THF, 2.0 equiv; for **a**: 27.2 mL, 13.6 mmol; or for **b**: 29.7 mL, 14.9 mmol) was added dropwise into the solution at 0 °C and stirred for 2 h. After the reaction has completed, degassed methanol (10 mL) was added to quench the excess sodium diphenylphosphide. Afterward, THF solvent was removed under vacuum, and the crude product was filtered through Celite using hexane as the eluent to remove NaCl salts. The filtrate was collected and further purified by silica-gel column chromatography using a mixture of hexane and dichloromethane (3:1 v/v) as eluent. The first yellow band was collected and concentrated under vacuum, yielding a red-orange oil product. For **1a**, R = $(CH_2)_4CH{=}CH_2$: Yield: 63%. $^{31}$P NMR ($CDCl_3$): −15.8 ppm (uncoordinated phosphine). $^1$H NMR ($CDCl_3$): 7.35 (m, 10H, $C_6H_5$), 5.81 (ddt, $J$ = 16.7 Hz, 9.0 Hz, 6.8 Hz, 1H, $CH{=}CH_2$), 4.94 (m, 2H, $CH{=}CH_2$), 4.56 (s, 2H, $C_5H_4$), 4.84 (s, 2H, $C_5H_4$), 2.34 (t, 2H, $CH_2PPh_2$), 2.05 (t, 2H, $(C_5H_4)CH_2$), 1.63 (m, 2H, $CH_2CH_2CH_2P$), 1.39 (m, 2H, $FeCH_2$), 1.26 (m, 6H, $CH_2(CH_2)_3CH{=}CH_2$) ppm. For **1b**, R = $(CH_2)_5CH_3$: Yield: 58%. $^{31}$P NMR ($CDCl_3$): −15.8 ppm (coordinated phosphine). $^1$H NMR ($CDCl_3$): 7.60−7.31 (m, 10H, $P(C_6H_5)_2$) 4.56 (s, 2H, $C_5H_4$), 4.48 (s, 2H, $C_5H_4$), 2.33 (t, 2H, $CH_2PPh_2$), 2.06 (t, 2H, $(C_5H_4)CH_2$), 1.85 (m, 2H, $CH_2CH_2CH_2P$), 1.36 (2H, Fe−$CH_2$) 1.25 (8H, $FeCH_2(CH_2)_4CH_3$), 0.86 (3H, $(CH_2)_5CH_3$) ppm.

**Synthesis of P($^P$FpR) Macrocycles, 2.** In a Schlenk flask containing **1** (1.0 g, 2.1 mmol, 70 wt % in THF), MIP was initiated by heating the reaction flask at an elevated temperature to 60 °C for 48 h. After 48 h, MIP was terminated by cooling the reaction flask to room temperature. The crude product was dissolved in a small amount of THF (5 mL) and precipitated into hexane (400 mL). The polymer was separated via filtration and washed with hexane 3 times to remove impurity traces. The isolated precipitates were dried under vacuum for 24 h, yielding yellow powders. For **2a**, R = $(CH_2)_4CH{=}CH_2$: Yield: 50%. $^{31}$P NMR ($CDCl_3$): 72.3 ppm. $^1$H NMR ($CDCl_3$): 7.45−7.25 (br, 10H, $C_6H_5$), 5.73 (m, 1H, $(CH_2)_4CH{=}CH_2$), 4.90 (m, 2H, $(CH_2)_4CH{=}CH_2$), 4.09−3.95 (m, 4H, $C_5H_4$), 2.78 (s, 1H, $Fe(CO)CH_2(CH_2)_3CH{=}CH_2$), 2.53 (s, 1H, $Fe(CO)CH_2(CH_2)_3CH{=}CH_2$), 2.25−2.11 (m, 4H, $CH_2CH_2CH_2PPh_2$), 1.92 (m, 2H, $CH_2CH_2CH_2PPh_2$), 1.45−1.18 (m, 6H, $Fe(CO)CH_2(CH_2)_3CH{=}CH_2$) ppm. For **2b**, R = $(CH_2)_5CH_3$: Yield: 48%. $^{31}$P NMR ($CDCl_3$): 72.4 ppm. $^1$H NMR ($CDCl_3$): 7.38−7.25 (br, 10H, $C_6H_5$), 4.08−3.95 (m, 4H, $C_5H_4$), 2.76 (s, 1H, $Fe(CO)CH_2(CH_2)_4CH_3$), 2.52 (s, 1H, $Fe(CO)CH_2(CH_2)_4CH_3$), 2.24−2.12 (m, 4H, $CH_2CH_2CH_2PPh_2$), 1.25−1.05 (br, 10H, $CH_2CH_2CH_2PPh_2$ and $Fe(CO)CH_2(CH_2)_4CH_3$), 0.83 (s, 3H, $Fe(CO)CH_2(CH_2)_4CH_3$) ppm.

**Synthesis of Intramolecular $^P$FpR Ring, 3.** In a Schlenk flask containing **1** (600 mg, 1.23 mmol, 1.0 wt % in THF), the solution was stirred at 60 °C for 48 h. The resulting solution was cooled to room temperature, and the THF solvent was removed under vacuum. The crude product was purified by silica gel column chromatography using a mixture of hexane and dichloromethane (3:1 v/v) as the eluent. The orange band was collected and concentrated under vacuum, yielding a bright orange oil product. For **3a**, R = $(CH_2)_4CH{=}CH_2$: Yield: 80%; red/orange oil. $^{31}$P NMR (300 MHz, $CDCl_3$): 71.5 ppm (s). $^1$H NMR (300 MHz, $CDCl_3$): 7.62 (m, 2H, $C_6H_5$), 7.39 (m, 3H, $C_6H_5$), 7.16 (m, 5H, $C_6H_5$), 5.69 (ddt, $J$ = 17.3, 10.2, and 6.5 Hz, 1H, $H_2C{-}CH{=}CH_2$), 4.86 (m, 2H, $-CH{=}CH_2$), 4.69 (s, 1H, $C_5H_4$), 4.60 (s, 1H, $C_5H_4$), 4.23 (s, 1H, $C_5H_4$), 3.94 (s, 1H, $C_5H_4$), 2.77 (tdd, $J$ = 13.6 Hz, 6.7 Hz, 2.1 Hz, 1H, $CH_2CH_2P$), 2.55 (m, 3H), 2.38 (m, 1H), 2.16 (m, 1H), 2.01 (m, 1H), 1.82 (m, 2H), 1.40 (m, 1H), 1.16 (m, 1H), 0.96 (m, 3H) ppm. $^{13}$C NMR (300 MHz, $CDCl_3$): 279.42 (d, $J$ = 25.22 Hz), 220.41 (d, $J$ = 28.31 Hz), 139.23 (s), 138.08 (d, $J$ = 46.64 Hz), 136.23 (d, $J$ = 38.87 Hz), 133.64 (s), 133.51 (s), 130.94 (s), 130.82 (s), 130.07 (s), 128.68 (s) 128.30 (s), 128.18 (s), 127.92 (s), 127.80 (s), 113.94 (s), 99.25 (s), 91.70 (s), 82.19 (s), 81.78 (s), 73.12 (s), 65.47 (d, $J$ = 5.5 Hz), 33.71 (s), 28.41 (s), 24.68 (s), 24.51 (s), 21.10 (s), 18.48 (d, $J$ = 26.43 Hz). ppm FT-IR: 1908 cm$^{-1}$ (terminal CO) and 1599 cm$^{-1}$ (acyl CO). ESI-MS: $m/z$ = 486.15, calculated for $C_{28}H_{31}FeO_2P$: 486.36. Anal. Calcd for $C_{28}H_{31}FeO_2P$: C 69.15, H 6.42. Found: C 62.86, H 6.62. (The discrepancy between the experimental and theoretical values is attributed to the low purity of the starting reagent of 6-chloro-1-hexene (96%)). For **3b**, R = $(CH_2)_5CH_3$: Yield: 83%; red/orange oil. $^{31}$P NMR (300 MHz, $CDCl_3$): 71.6 ppm. $^1$H NMR (300 MHz, $CDCl_3$): 7.61 (s, 2H, $C_6H_5$), 7.39 (s, 3H, $C_6H_5$), 7.16 (m, 5H, $C_6H_5$), 4.68 (s, 1H, $C_5H_4$), 4.60 (s, 1H, $C_5H_4$), 4.24 (s, 1H, $C_5H_4$), 3.94 (s, 1H, $C_5H_4$), 2.78 (tdd, $J$ = 13.6 Hz, 6.8 Hz, 2.3 Hz, 1H, $CH_2CH_2P$), 2.54 (m, 3H), 2.37 (m, 1H), 2.17 (m, 1H), 1.99 (m, 1H), 1.40 (m, 1H), 1.14 (m, 3H), 1.02 (m, 3H), 0.86 (m, 2H), 0.79 (m, 3H, $CH_2CH_3$) ppm. $^{13}$C NMR (300 MHz, $CDCl_3$): 279.58 (d, $J$ = 28.11 Hz), 220.46 (d, $J$ = 28.11 Hz), 138.16 (d, $J$ = 49.20 Hz), 136.42 (d, $J$ = 38.65 Hz), 133.69 (s), 133.53 (s), 130.95 (s), 130.84 (s), 130.05 (s), 128.64 (s), 128.34 (s), 128.17 (s), 127.90 (s), 127.77 (s), 99.25 (s), 91.65 (s), 82.20 (s), 81.77 (s), 73.12 (s), 65.81 (d, $J$ = 5.27 Hz), 31.74 (s), 28.77 (s), 24.90 (s), 24.68 (s), 22.53 (s), 21.13 (s), 18.50 (d, $J$ = 29.8 Hz), 14.08 (s) ppm. FT-IR: 1906 cm$^{-1}$ (terminal CO) and 1596 cm$^{-1}$ (acyl CO). ESI-MS: $m/z$ = 488.16, calculated for $C_{28}H_{33}FeO_2P$: 488.38. Anal. Calcd for $C_{28}H_{33}FeO_2P$: C 68.86, H 6.81. Found: C 68.76, H 6.86.

## ■ ASSOCIATED CONTENT

### Supporting Information

The Supporting Information is available free of charge at https://pubs.acs.org/doi/10.1021/acs.organomet.0c00346.

Characterization data including NMR spectra and X-ray crystallographic data for compounds **3a** and **3b** (PDF)

### Accession Codes

CCDC 1955716 and 1955718 contain the supplementary crystallographic data for this paper. These data can be obtained free of charge via www.ccdc.cam.ac.uk/data_request/cif, or by emailing data_request@ccdc.cam.ac.uk, or by contacting The Cambridge Crystallographic Data Centre, 12 Union Road, Cambridge CB2 1EZ, UK; fax: +44 1223 336033.

## ■ AUTHOR INFORMATION


### Corresponding Author

**Xiaosong Wang** − *Department of Chemistry and Waterloo Institute for Nanotechnology (WIN), University of Waterloo, Waterloo, Ontario N2L 3G1, Canada;* orcid.org/0000-0002-6415-4768; Email: xiaosong.wang@uwaterloo.ca

### Authors

**Aaron Leung** − *Department of Chemistry and Waterloo Institute for Nanotechnology (WIN), University of Waterloo, Waterloo, Ontario N2L 3G1, Canada*

**Jing Kang** − *Department of Chemistry and Waterloo Institute for Nanotechnology (WIN), University of Waterloo, Waterloo, Ontario N2L 3G1, Canada; State Key Laboratory of Supramolecular Structure and Materials, College of Chemistry, Jilin University, Changchun 130012, Jilin, China*

**Yuanting Cai** − *Department of Chemistry and Waterloo Institute for Nanotechnology (WIN), University of Waterloo, Waterloo, Ontario N2L 3G1, Canada; State Key Laboratory of Physical Chemistry of Solid Surfaces and Collaborative Innovation Centre of Chemistry for Energy Materials (iChEM), College of Chemistry and Chemical Engineering, Xiamen University, Xiamen 261005, Fujian, China*

**Weiwei Chang** − *Department of Chemistry and Waterloo Institute for Nanotechnology (WIN), University of Waterloo,*




https://dx.doi.org/10.1021/acs.organomet.0c00346
Organometallics 2020, 39, 2991−2997

*Waterloo, Ontario N2L 3G1, Canada; Analysis and Testing Center, Shandong University of Technology, Zibo 255049, Shandong, China*

**Kun Liu** − *State Key Laboratory of Supramolecular Structure and Materials, College of Chemistry, Jilin University, Changchun 130012, Jilin, China;* orcid.org/0000-0003-2940-9814

**Haiping Xia** − *State Key Laboratory of Physical Chemistry of Solid Surfaces and Collaborative Innovation Centre of Chemistry for Energy Materials (iChEM), College of Chemistry and Chemical Engineering, Xiamen University, Xiamen 261005, Fujian, China;* orcid.org/0000-0002-2688-6634

Complete contact information is available at: https://pubs.acs.org/10.1021/acs.organomet.0c00346

### Notes

The authors declare no competing financial interest.

## ■ ACKNOWLEDGMENTS

We would like to acknowledge the financial support of the Natural Sciences and Engineering Research Council of Canada (NSERC) [50503-10556].

## ■ REFERENCES

(1) Williams, R. J.; Dove, A. P.; O'Reilly, R. K. Self-assembly of cyclic polymers. *Polym. Chem.* **2015**, *6*, 2998−3008.
(2) Hass, H. B.; McBee, E. T.; Hinds, G. E. Synthesis of Cyclopropane. *Ind. Eng. Chem.* **1936**, *28*, 1178−1181.
(3) Steed, J. W. First- and Second-Sphere Coordination Chemistry of Alkali Metal Crown Ether Complexes. *Coord. Chem. Rev.* **2001**, *215*, 171−221.
(4) Herbert, D. E.; Gilroy, J. B.; Chan, W. Y.; Chabanne, L.; Staubitz, A.; Lough, A. J.; Manners, I. Redox-Active Metallomacrocycles and Cyclic Metallopolymers: Photocontrolled Ring-Opening Oligomerization and Polymerization of Silicon-Bridged [1]-Ferrocenophanes Using Substitutionally-Labile Lewis Bases as Initiators. *J. Am. Chem. Soc.* **2009**, *131*, 14958−14968.
(5) Tu, X.; Liu, M.; Wei, H. Recent progress on cyclic polymers: Synthesis, bioproperties, and biomedical applications. *J. Polym. Sci., Part A: Polym. Chem.* **2016**, *54*, 1447−1458.
(6) Tseng, Y.-Y.; Kamikawa, K.; Wu, Q.; Takahashi, T.; Ogasawara, M. Ring-Closing Metathesis of ($\eta^5$-Alkenylcyclopentadienyl)(alkenylphosphine)manganese(I) Dicarbonyl Complexes. *Adv. Synth. Catal.* **2015**, *357*, 2255−2264.
(7) Ogasawara, M.; Nagano, T.; Hayashi, T. Metathesis Route to Bridged Metallocenes. *J. Am. Chem. Soc.* **2002**, *124*, 9068−9069.
(8) Kohser, S.; Butenschon, H. (Di-*tert*-butylphosphanylethyl)-cyclopentadienylnickel Chelates with Alkyl, Alkenyl, Aryl, and Alkynyl Ligands: Hints to Cumulenylidene Resonance Forms. *Eur. J. Inorg. Chem.* **2018**, *2018*, 31−45.
(9) Ceccon, A.; Santi, S.; Orian, L.; Bisello, A. Electronic communication in heterobinuclear organometallic complexes through unsaturated hydrocarbon bridges. *Coord. Chem. Rev.* **2004**, *248*, 683−724.
(10) Herbert, D. E.; Mayer, U. F. J.; Manners, I. Strained metallocenophanes and related organometallic rings containing pi-hydrocarbon ligands and transition-metal centers. *Angew. Chem., Int. Ed.* **2007**, *46*, 5060−5081.
(11) Pannell, K. H.; Sharma, H. K. (Cyclopentadienyl)-dicarbonylmethyliron (($\eta^5$-$C_hH_5$)$Fe(CO)_2CH_3$, FpMe), a Seminal Transition-Metal Alkyl Complex: Mobility of the Methyl Group. *Organometallics* **2010**, *29*, 4741−4745.
(12) Butenschon, H. Cyclopentadienylmetal Complexes Bearing Pendant Phosphorus, Arsenic, and Sulfur Ligands. *Chem. Rev.* **2000**, *100*, 1527−1564.
(13) Bellabarba, R. M.; Nieuwenhuyzen, M.; Saunders, G. C. Intramolecular $S_NAr$ reactions as a route to complexes of hybrid cyclopentadienyl-phosphine ligands: synthesis of a rhodium complex of the first $\eta^5$, $\eta^1$, $\eta^1$-cyclopentadienyl-phosphine-thioether ligand. *J. Chem. Soc., Dalton Trans.* **2001**, 512−514.
(14) Bentz, K. C.; Cohen, S. M. Supramolecular Metallopolymers: From Linear Materials to Infinite Networks. *Angew. Chem., Int. Ed.* **2018**, *57*, 14992−15001.
(15) Wang, X.; Cao, K.; Liu, Y.; Tsang, B.; Liew, S. Migration Insertion Polymerization (MIP) of Cyclopentadienyldicarbonyldiphenylphosphinopropyliron (FpP): A New Concept for Main Chain Metal-Containing Polymers (MCPs). *J. Am. Chem. Soc.* **2013**, *135*, 3399−3402.
(16) Cao, K.; Peng, L.; Zhu, J.; Feng, A.; Liu, D.; Worku, A.; Liu, S.; Lin, J.; Yuan, J.; Wang, X. Chain-Conformation-Directed Polymerization Cyclization for Effective Synthesis of Macrocycles in Bulk. *Chem. - Eur. J.* **2018**, *24*, 15380−15386.
(17) Inkpen, M. S.; Scheerer, S.; Linseis, M.; White, A. J. P.; Winter, R. F.; Albrecht, T.; Long, N. J. Oligomeric ferrocene rings. *Nat. Chem.* **2016**, *8*, 825−830.
(18) Musgrave, R. A.; Russell, A. D.; Hayward, D. W.; Whittell, G. R.; Lawrence, P. G.; Gates, P. J.; Green, J. C.; Manners, I. Main-chain metallopolymers at the static-dynamic boundary based on nickelocene. *Nat. Chem.* **2017**, *9*, 743−750.
(19) Kunz, K.; Erker, G.; Doring, S.; Frohlich, R.; Kehr, G. Generation of Homogeneous ($sp^3$-$C_1$)-Bridged Cp/Amido and Cp/Phosphido Group 4 Metal Ziegler-Natta Catalyst Systems. *J. Am. Chem. Soc.* **2001**, *123*, 6181−6182.
(20) McConnell, A. C.; Pogorzelec, P. J.; Slawin, A. M. Z.; Williams, G. L.; Elliott, P. I. P.; Haynes, A.; Marr, A. C.; Cole-Hamilton, D. J. The synthesis, characterisation and reactivity of 2-phosphanylethylcyclopentadienyl complexes of cobalt, rhodiuim and iridium. *Dalton Trans.* **2006**, No. 1, 91−107.
(21) Nicholas, K.; Raghu, S.; Rosenblum, M. Intermediates in the intramolecular ligand transfer reactions of $\eta^5$-$C_5H_5Fe(CO)_2R$ complexes. *J. Organomet. Chem.* **1974**, *78*, 133−137.
(22) Cao, K.; Ward, J.; Amos, R. C.; Jeong, M. G.; Kim, K. T.; Gauthier, M.; Foucher, D.; Wang, X. Organometallic macromolecules with piano stool coordination repeating units: chain configuration and stimulated solution behavior. *Chem. Commun.* **2014**, *50*, 10062−10065.
(23) Liu, J.; Guan, Z.; Tian, X.; Lin, J.; Wang, X. Solvent-dependent chain conformation for ring closure of metal carbonyl oligomers *via* migration insertion polymerization (MIP) of $CpFe(CO)_2(CH_2)_6PPh_2$. *Polym. Chem.* **2016**, *7*, 4419−4426.
(24) Cao, K.; Tsang, B.; Liu, Y.; Chelladural, D.; Power, W. P.; Wang, X. Synthesis, Cyclization, and Migration Insertion Oligomerization of $CpFe(CO)_2(CH_2)_3PPh_2$ in Solution. *Organometallics* **2014**, *33*, 531−539.
(25) Chalaris, M.; Marinakis, S.; Dellis, D. Temperature effects on the structure and dynamics of liquid dimethyl sulfoxide: A molecular dynamics study. *Fluid Phase Equilib.* **2008**, *267*, 47−60.
(26) Ciocirlan, O.; Iulian, O. Vapor pressure, density, viscosity and refractive index of dimethyl sulfoxide + 1,4-dimethylbenzene system. *J. Serb. Chem. Soc.* **2008**, *73*, 73−85.
(27) Josse, T.; De Winter, J.; Gerbaux, P.; Coulembier, O. Cyclic Polymers by Ring-Closure Strategies. *Angew. Chem., Int. Ed.* **2016**, *55*, 13944−13958.

## ■ NOTE ADDED AFTER ASAP PUBLICATION

This paper was published ASAP on August 7, 2020, with incorrect versions of Scheme 1 and Figure 8. The corrected version was reposted on August 24, 2020.



https://dx.doi.org/10.1021/acs.organomet.0c00346
*Organometallics* 2020, 39, 2991−2997